Generation of Isolated Subfemtosecond Electron Bunches by the Diffraction of a Polarization-Tailored Intense Laser Beam

Ke Hu[1,2] and Longqing Yi[1,2,3,*]

[1]Tsung-Dao Lee Institute, Shanghai Jiao Tong University, Shanghai 201210, China
[2]Collaborative Innovation Center of IFSA (CICIFSA), Shanghai Jiao Tong University, Shanghai 200240, China
[3]Key Laboratory for Laser Plasmas (Ministry of Education), School of Physics and Astronomy, Shanghai Jiao Tong University, Shanghai 200240, China

(Received 15 March 2024; accepted 24 June 2024; published 23 July 2024)

We propose utilizing a polarization-tailored high-power laser pulse to extract and accelerate electrons from the edge of a solid foil target to produce isolated subfemtosecond electron bunches. The laser pulse consists of two orthogonally polarized components with a time delay comparable to the pulse duration, such that the polarization in the middle of the pulse rapidly rotates over 90° within few optical cycles. Three-dimensional particle-in-cell simulations show that when such a light pulse diffracts at the edge of a plasma foil, a series of isolated relativistic electron bunches are emitted into separated azimuthal angles determined by the varying polarization. In comparison with most other methods that require an ultrashort drive laser, we show the proposed scheme works well with typical multicycle (∼30 fs) pulses from high-power laser facilities. The generated electron bunches have typical durations of a few hundred attoseconds and charges of tens of picocoulombs.

DOI: 10.1103/PhysRevLett.133.045001

The production of subfemtosecond electron bunches has become a research focus because of its diverse applications, such as ultrafast electron imaging [1,2], electron diffraction and microscopy [3–6]. Such beams can serve as secondary sources for radiation production down to attosecond level [7–11]. There have been extensive studies on generating relativistic attosecond electron bunches using nonlinear interaction between an intense femtosecond laser pulse and matter, both theoretical [12–14] and experimental [5,15]. However, the generated electron beam typically consists of a train of bunches. The generation of isolated ultrashort electron bunches (IUEB) reaching subfemotosecond timescale remains challenging [6], especially in the high-energy range, which is of particular interest for single shot ultrafast experiments. Moreover, most current numerical approaches rely on interactions between a few-cycle driving laser pulse and a nanoscaled target, such as a droplet [16], a nanotip [17], or an ultrathin foil [10,18]. The drive laser typically has a full width at half maximum (FWHM) duration smaller than 5 fs, ensuring that only one optical cycle is sufficiently strong to extract a considerably populated bunch from the target.

In this Letter, we demonstrate that the generation of IUEBs can be achieved by the diffraction of an intense polarization-tailored laser pulse at the edge of a solid foil. The drive laser is multicycle, which is available in most high-power facilities. It is linearly polarized in orthogonal directions at both ends, and in the middle the polarization direction rapidly rotates over 90° within a few optical cycles [Fig. 1(a)]. Such pulses can be routinely produced by the polarization gating technique [19–21], where a quartz plate is used to split a linearly polarized laser pulse into two orthogonally polarized components, with an adjustable delay by varying the thickness of the plate. When such a laser shines at the overdense plasma edge, relativistic electrons are accelerated via vacuum laser acceleration (VLA) [22,23], with the emission angles controlled by the laser polarization. Thus, attosecond electron bunches are produced in each laser cycle from the middle of the pulse, but emitted in slightly different angles, analogous to the "attosecond lighthouse" [24,25], except that the emission angle is controlled by a rotating polarization instead of the wave front direction.

The sketch of our simulation setup is illustrated in Fig. 1(b), the simulation is performed with three-dimensional (3D) particle-in-cell (PIC) simulations with the EPOCH code [26]. A polarization-tailored drive laser pulse traveling along the x direction is focused onto the edge of a solid foil target. The laser focus spot is partially blocked by the foil, which leads to diffraction. The laser field is given as

$$\begin{aligned}\mathbf{E} = &\exp[-(y^2+z^2)^2/w_0^2] \\ &\times \{\mathbf{e_y} E_1 \exp(-t^2/T^2)\exp(ik_0x - i\omega_0 t) \\ &+ \mathbf{e_z} E_2 \exp[-(t-\Delta t)^2/T^2]\exp(ik_0x - i\omega_0 t + \varphi)\}. \end{aligned} \quad (1)$$

*Contact author: lqyi@sjtu.edu.cn

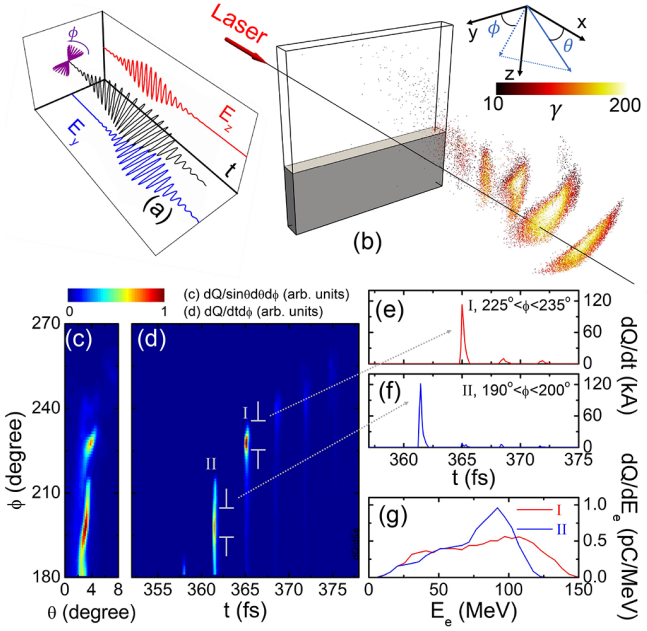

FIG. 1. (a) Electric field of the polarization-tailored drive laser in E_y-E_z-t space and its projections on E_y-t, E_z-t, and E_z-E_y planes. (b) 3D schematic setup of the proposed scheme. The orange dots are fast electrons ($\gamma > 10$) at simulation time $t = 120\tau_0$ and the color represents their energies. Density distribution of fast electrons are shown in ϕ-θ space (c) and ϕ-t space (d). Currents of (e) bunch I and (f) bunch II are obtained by selecting out electrons within a certain range of the azimuthal angle [gray area in (d)]. (g) Energy spectra of bunches I and II.

One can see that the laser is consisted of two orthogonally polarized components with amplitudes E_1 and E_2, denoted by unit vectors $\mathbf{e_y}$ and $\mathbf{e_z}$. Here we first consider the case with $E_1 = E_2$, and the normalized amplitudes are $a_1 = a_2 = eE_1/mc\omega_0 = 10$ (corresponding to a laser intensity 1.37×10^{20} W/cm^2), where ω_0 is the angular frequency, c is the speed of light, m is the electron mass, and e is the unit charge. The laser wavelength is $\lambda_0 = 1$ μm, $k_0 = 2\pi/\lambda_0$ is the wave number, $\tau_0 = \lambda_0/c$ is the laser period, and $w_0 = 12$ μm is the laser spot size. The two laser components, each has a FWHM duration of 20.0 fs ($T = 17.0$ fs) are separated by a time delay of $\Delta t = 23.3$ fs. The relative phase difference is set to be $\varphi = 0$ here, its effects will be discussed later. We note the proposed scheme is insensitive to finite oblique incident angle, polarization misalignment, as well as speckled pulses, as detailed in Supplemental Material [27].

The foil target is modeled by a 1-μm thick (in the x direction) preionized plasma slab, and the density is $n_0 = 50n_c$, where $n_c = \epsilon_0 m\omega_0^2/e^2$ is the critical density. The foil is place at $z > z_0 = 4.4$ μm, with a density ramp at the boundary to account for plasma expansion due to the laser prepulse: $n(z) = n_0 \exp[(z - z_0)/\sigma_0]$ for $z < z_0$, where the sale length is $\sigma_0 = 0.1$ μm. The simulation box has dimensions of $x \times y \times z = 32 \times 30 \times 30$ μm^3 and is sampled by $1280 \times 1200 \times 1200$ cells, and a moving window is used to simulate the electron propagation over a long distance. For the primary simulation presented in Fig. 1, the number of macroparticles per cell (NPC) for electrons is set to be 100 to test numerical convergence and ensure the generated IUEBs are properly resolved. In the following simulations, a reduced NPC is used (16) to improve computational efficiency.

When there is a sufficiently strong laser electric field component perpendicular to the plasma-vacuum boundary, the diffraction of a relativistic laser can produce a train of fast electron bunches [12]. In our simulation, the edge of the target is parallel to the laser polarization in the leading half. Then the laser polarization rotates over 90° to the perpendicular direction (E_z), thus electrons can be extracted out of the foil and accelerated.

The electron bunches, recorded at 100 μm away from the target are shown as orange dots in Fig. 1(b). Their distributions in ϕ-θ space (divergence), and ϕ-t space are illustrated in Figs. 1(c) and 1(d), where θ and ϕ are defined in Fig. 1(b). Notably, all the electron bunches are forward directed, concentrated within a small opening angle $d\theta \approx 1°$ centered around $\theta \approx 3°$. On the other hand, the azimuthal angles of the accelerated electrons are strongly dependent on the instantaneous polarization, which is rapidly rotating. As shown by Fig. 1(d), two main electron bunches are generated with an azimuthal angle separation of $\Delta\phi_s \approx 30°$. Notably, this separation exceeds the azimuthal divergence observed within each individual bunch ($\Delta\phi_b \approx 8°$ and 20° for the two bunches). Therefore, IUEBs can be obtained by collecting the electrons within certain ranges of the azimuthal angle.

Electrons that peak around $\phi = 235°$ and 195° are selected out and denoted as bunch I and bunch II, and the beam current of electrons centered within 10° around each peak are plotted in Figs. 1(e) and 1(f). The temporal FWHM duration of bunches I and II are 250 and 200 as, with total charges of 38.6 and 37.5 pC, respectively, on the same order of magnitude as reported in other numerical studies [10,16,17]. This results in an averaged current of 139.71 kA for bunch I and 187.23 kA for bunch II. Figure 1(g) shows the broad energy spectra of the two bunches, as can be expected from the VLA mechanism. The maximum energies are 145.4 MeV for bunch I and 124.7 MeV for bunch II, the averaged electron energy are around 70 MeV for both bunches. Thus, the mean current of the IUEB reach ~10% of the Alfvén limit.

To produce such an ultrashort dense electron bunch, it is crucial to accelerate the electrons to relativistic energy as fast as possible, so that beam loading and the longitudinal spread of the beam is reduced by the relativistic effects, which decrease the expelling forces by γ^{-2} [28].

In the present scheme, the diffraction of the drive laser beam can boost the electron energy significantly, as shown by Fig. 2(a). By tracking the trajectories of electrons in bunch I, we can see that a brief but strong acceleration

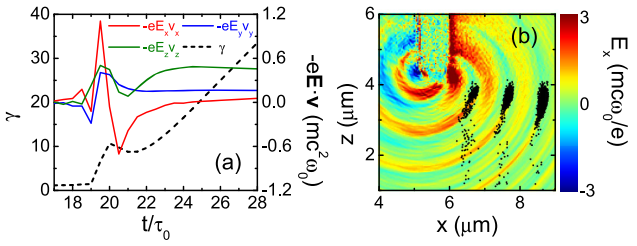

FIG. 2. Electron energy boost by the diffracted laser field. (a) Average γ factor and the instantaneous work done by each electric field components plotted against time at the early stage of acceleration. (b) Distribution of fast electrons ($\gamma > 5$) on the x-z plane at $t = 21\tau_0$. On the background is a snapshot of E_x at the same moment.

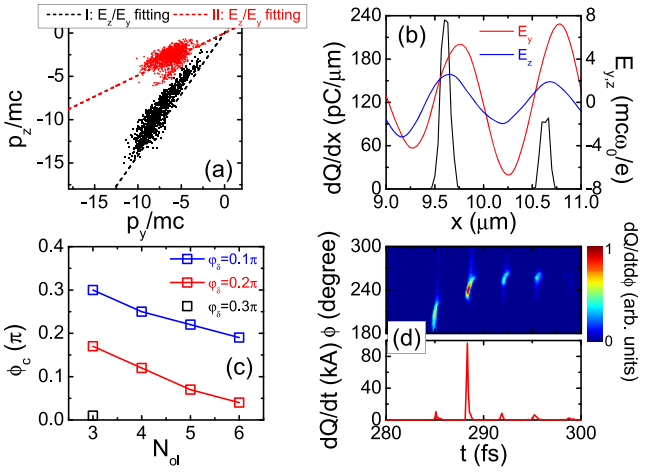

FIG. 3. (a) Electron distributions of bunches I and II in p_y-p_z space at $t = 80\tau_0$. Each dashed line represents a linear fit of the ratio of the electric field acting on the corresponding electrons in the z and y directions. (b) Waveforms of E_y and E_z, and density profile of the fast electrons at $t = 22\tau_0$. The relative phase is $\varphi = 0.15\pi$. (c) Critical phase mismatch ϕ_c versus the number of overlapping optical cycles N_{ol} for different bunch duration. (d) IUEB production with $\varphi = 0.2\pi$. Upper: density distribution of fast electrons in ϕ-t space. Lower: current of the IUEB (electrons within $235° < \phi < 245°$).

phase boosts the electron energy to $\gamma \sim 10$ during laser diffraction. Then, the electrons are accelerated mainly by the VLA mechanism in a second, much longer stage, with moderate acceleration gradient.

In the first stage, the main contribution comes from the strong longitudinal component E_x of the near-field diffracted light [Fig. 2(b)]. The electrons are injected into the accelerating phase, with velocities predominately along the x direction, thus experience an acceleration gradient comparable to the drive laser field, which is roughly 3× higher than that in the VLA stage. Then, a short deceleration occurs, as the electrons cannot keep up with the accelerating phase. Nevertheless, since the diffracted laser beam disperses very quickly, the E_x field is much weaker when dephasing occurs. Therefore, a net energy gain can be expected. When the electrons are sufficiently far away from the target, the electromagnetic field is essentially a planar wave, so that VLA takes over.

We note that the ability to angularly control electron acceleration using a polarization-tailored drive laser beam is a unique advantage of the relativistic laser diffraction process. In comparison, when such a laser is reflected by a foil target [23,29], the superposition of incident and reflected laser fields form a complex structure near the target surface, which hinders electron emission in the direction parallel to the target surface. Therefore, the accelerated electrons form two bunch trains on the incident plane (see Supplemental Material [27]).

In the following, we consider the condition under which the IUEB can be produced. Namely, the divergence of each electron bunch should be smaller than the bunch separation angle, $\Delta\phi_b < \Delta\phi_s \approx \pi/2N_{ol}$, where $N_{ol} \approx (2T - \Delta t)/\tau_0$ is the number of overlapping optical cycles.

The VLA mechanism follows the conservation of canonical momentum in transverse direction $\mathbf{p}_\perp = e\mathbf{A}/c$ [30], where $\mathbf{A}$ is the vector potential satisfying $\mathbf{A} = -\partial\mathbf{E}/\partial t$. The azimuthal angle of the electrons is determined by the electric fields $\phi_b(t) = \arctan[E_z(t)/E_y(t)]$, since $E_z/E_y = A_z/A_y$. Apparently, this value varies in each optical cycle in the polarization-rotating region of the drive laser. As a result, the electrons in bunches I and II [Fig. 1(d)] form two distinguished peaks in transverse momentum space p_y-p_z, marked by black and red dots in Fig. 3(a), respectively, which can be fitted by the ratio of instantaneous electric fields act on them.

The azimuthal divergence of each bunch $\Delta\phi_b$ can be obtained by considering the variation of E_y and E_z components within the bunch duration δ_b. This is predominately determined by δ_b and the relative phase difference (φ) between E_y and E_z components. The electrons are injected within a narrow phase close to the peak of the laser electric field perpendicular to the diffraction edge (E_z) in each optical cycle, this can be seen from Fig. 3(b), where the relative phase between the E_y and E_z fields is $\varphi = 0.15\pi$. The divergence of the electron bunches can be obtained as $\Delta\phi_b \approx \arctan[1/\cos(\varphi + \varphi_\delta)] - \arctan(\cos\varphi_\delta)$, where $\varphi_\delta = 2\pi\delta_b/\tau_0$ is corresponding to the accelerating phase occupied by the electron bunch. Here we have approximately set the ratio of local E_z/E_y to be unity, which can be justified by our PIC simulations.

Because of the ultrashort nature of subfemtosecond bunches, φ_δ is typically quite small ($< 0.2\pi$). It is easy to see that $\Delta\phi_b$ is in minimum when $\varphi = 0$ and increases with φ. In reality, it is very challenging to manipulate the relative phase between E_y and E_z, as it requires subcycle level temporal precision.

Fortunately, we can demonstrate that by controlling N_{ol}, our scheme works with a substantial range of nonzero ϕ. The results are summarized in Fig. 3(c), where the blue,

red, and black curves show the evolution of critical phase mismatch φ_c, below which the IUEBs can be produced, as a function of N_{ol} for electron bunch length of 166.7, 333.3, and 500 as, respectively. Here we only consider $0 \le \varphi < \pi/2$, for $\pi/2 \le \varphi < \pi$, the results are the same, except the IUEBs are emitted into a different quadrant in the y-z plane.

As one can see, it is in general more resilient against wider ranges of phase mismatch for shorter electron bunches. Importantly, we show by reducing N_{ol}, φ_c increases significantly, meaning a higher tolerance for the phase difference. According to our simulations, δ_b is typically 100–300 as, corresponding to $\varphi_c \sim 0.2\pi - 0.3\pi$. An example is presented in Fig. 3(d), where two 15.7-fs mutual orthogonally polarized pulses are separated by $\Delta t = 5\tau_0$ ($N_{ol} = 3$), an isolated 200-as electron bunch is produced with $\varphi = 0.2\pi$.

It is important to note that N_{ol} cannot be arbitrarily small for a given laser duration. In particular, when the duration is long, a small N_{ol} may cause the intensity of the drive laser beam in the polarization-tailored region too weak to extract electrons out of the plasma target. In this work, we restrict ourselves to laser durations $T > 15$ fs and $N_{ol} > 3$.

Finally, we consider the preheating effect which leads to a non-negligible initial electron momenta ($\mathbf{p}_{\perp,\mathbf{0}}$) before they are pulled out by the laser. In this study, the preheating is mostly caused by the first half of the main laser pulse, which leads to "$\mathbf{J} \times \mathbf{B}$" heating [31] or vacuum heating [32] of the target electrons. This effect becomes increasingly important as the laser duration becomes longer. Here we neglect the heating by the laser prepulse as the energy in the prepulse is much lower than the main pulse for a reasonably high-contrast laser beam.

The VLA stage satisfies $\mathbf{p}_\perp = \mathbf{p}_{\perp,\mathbf{0}} + e\mathbf{A}/c$ when considering the initial momenta. As discussed before, the second term ($e\mathbf{A}/c$) is quite similar for all the electrons in the same bunch, since the width of the electron bunch is much shorter compared to the laser optical cycle, but a boarder range of $\mathbf{p}_{\perp,\mathbf{0}}$ distribution can significantly increase the azimuthal angular divergence of the bunches, making it harder to separate them from each other. As shown in Fig. 4(a), where we consider a longer laser pulse with $T = 7\tau_0$ and $\Delta t = 10\tau_0$ ($N_{ol} \approx 4$) (other parameters are the same as in Fig. 1), the angular divergence is $\Delta\phi_b \sim 30°$.

Nevertheless, the preheating effect can be mitigated by reducing the intensity of the leading-half component, as shown by Fig. 4(b). When we set $a_1 = 5$, $a_2 = 10$, one can see the azimuthal beam divergence is significantly reduced ($\Delta\phi_b \sim 10°$) comparing to Fig. 4(a). This can be easily understood as the leading half of the drive laser beam is weaker, thus the plasma temperature is lower, the accelerated electrons tend to follow the same trajectory. Therefore, the intensity ratio between two laser components a_2/a_1 provides an additional degree of freedom to control the electron emission. In the case presented in Fig. 4(b), the IUEB has a charge of 27.8 pC, a duration of 300 as, an averaged beam current of 92.7 kA, which are comparable to the case presented in Fig. 1.

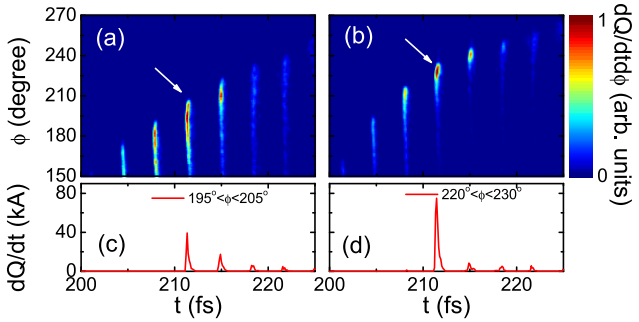

FIG. 4. PIC simulations on the preheating effect. Density distributions of fast electrons for $a_1 = a_2 = 10$ (a), and $a_1 = 5$, $a_2 = 10$ (b) are plotted in ϕ-t space. (c),(d) Currents of the IUEBs, selected from the electron bunches indicated by the arrows in (a) and (b), respectively.

In summary, our study demonstrates the generation of isolated subfemtosecond electron bunches with charge at 10-pC level when a polarization-tailored femtosecond laser beam diffracts at the edge of a solid foil. The extracted electrons are first boosted to relativistic energies by the near-field diffracted laser field, and then accelerated by the laser fields with tailored polarization, emitting into separated azimuthal angles. The number of overlapping optical cycles between two orthogonally polarized components, as well as their intensity ratio, provide two major degrees of freedom to control the electron emission process. The proposed scheme can work with a much longer laser duration compared with most other laser-plasma sources of isolated subfemtosecond electron bunches.

Acknowledgments—This work is supported by the National Key R&D Program of China (No. 2021YFA1601700), and the National Natural Science Foundation of China (No. 12205187).

[1] P. Baum and A. H. Zewail, 4D attosecond imaging with free electrons: Diffraction methods and potential applications, Chem. Phys. **366**, 2 (2009).
[2] D. Shorokhov and A. H. Zewail, Perspective: 4D ultrafast electron microscopy-evolutions and revolutions, J. Chem. Phys. **144**, 080901 (2016).
[3] K. E. Priebe, C. Rathje, S. V. Yalunin, T. Hohage, A. Feist, S. Schäfer, and C. Ropers, Attosecond electron pulse trains and quantum state reconstruction in ultrafast transmission electron microscopy, Nat. Photonics **11**, 12 (2017).
[4] M. T. Hassan, Attomicroscopy: From femtosecond to attosecond electron microscopy, J. Phys. B **51**, 032005 (2018).

[5] Y. Morimoto and P. Baum, Diffraction and microscopy with attosecond electron pulse trains, Nat. Phys. **14**, 252 (2018).
[6] D. Hui, H. Alqattan, M. Sennary, N. V. Golubev, and M. T. Hassan, Attosecond electron microscopy, arXiv:2305.03014.
[7] W. Luo, H. B. Zhuo, Y. Y. Ma, Y. M. Song, Z. C. Zhu, T. P. Yu, and M. Y. Yu, Attosecond Thomson-scattering x-ray source driven by laser-based electron acceleration, Appl. Phys. Lett. **103**, 174103 (2013).
[8] X.-L. Zhu, M. Chen, T.-P. Yu, S.-M. Weng, L.-X. Hu, P. McKenna, and Z.-M. Sheng, Bright attosecond γ-ray pulses from nonlinear Compton scattering with laser-illuminated compound targets, Appl. Phys. Lett. **112**, 174102 (2018).
[9] H.-C. Wu, J. Meyer-ter-Vehn, J. Fernández, and B. M. Hegelich, Uniform laser-driven relativistic electron layer for coherent Thomson scattering, Phys. Rev. Lett. **104**, 234801 (2010).
[10] H.-C. Wu, J. Meyer-ter-Vehn, B. M. Hegelich, and J. C. Fernández, Nonlinear coherent Thomson scattering from relativistic electron sheets as a means to produce isolated ultrabright attosecond x-ray pulses, Phys. Rev. ST Accel. Beams **14**, 070702 (2011).
[11] B. Dromey *et al.*, Coherent synchrotron emission from electron nanobunches formed in relativistic laser-plasma interactions, Nat. Phys. **8**, 804 (2012).
[12] N. Naumova, I. Sokolov, J. Nees, A. Maksimchuk, V. Yanovsky, and G. Mourou, Attosecond electron bunches, Phys. Rev. Lett. **93**, 195003 (2004).
[13] K. I. Popov, V. Yu. Bychenkov, W. Rozmus, R. D. Sydora, and S. S. Bulanov, Vacuum electron acceleration by tightly focused laser pulses with nanoscale targets, Phys. Plasmas **16**, 053106 (2009).
[14] T. V. Liseykina, S. Pirner, and D. Bauer, Relativistic attosecond electron bunches from laser-illuminated droplets, Phys. Rev. Lett. **104**, 095002 (2010).
[15] C. M. S. Sears *et al.*, Production and characterization of attosecond electron bunch trains, Phys. Rev. ST Accel. Beams **11**, 061301 (2008).
[16] V. Horný and L. Veisz, Generation of single attosecond relativistic electron bunch from intense laser interaction with a nanosphere, Plasma Phys. Control. Fusion **63**, 125025 (2021).
[17] D. E. Cardenas, T. M. Ostermayr, L. Di Lucchio, L. Hofmann, M. F. Kling, P. Gibbon, J. Schreiber, and L. Veisz, Sub-cycle dynamics in relativistic nanoplasma acceleration, Sci. Rep. **9**, 7321 (2019).
[18] V. Kulagin, V. Cherepenin, M. Hur, and H. Suk, Theoretical investigation of controlled generation of a dense attosecond relativistic electron bunch from the interaction of an ultrashort laser pulse with a nanofilm, Phys. Rev. Lett. **99**, 124801 (2007).
[19] P. B. Corkum, N. H. Burnett, and M. Y. Ivanov, Subfemtosecond pulses, Opt. Lett. **19**, 1870 (1994).
[20] O. Tcherbakoff, E. Mével, D. Descamps, J. Plumridge, and E. Constant, Time-gated high-order harmonic generation, Phys. Rev. A **68**, 043804 (2003).
[21] I. J. Sola *et al.*, Controlling attosecond electron dynamics by phase-stabilized polarization gating, Nat. Phys. **2**, 319 (2006).
[22] G. Malka, E. Lefebvre, and J. L. Miquel, Experimental observation of electrons accelerated in vacuum to relativistic energies by a high-intensity laser, Phys. Rev. Lett. **78**, 3314 (1997).
[23] M. Thévenet, A. Leblanc, S. Kahaly, H. Vincenti, A. Vernier, F. Quéré, and J. Faure, Vacuum laser acceleration of relativistic electrons using plasma mirror injectors, Nat. Phys. **12**, 355 (2016).
[24] H. Vincenti and F. Quéré, Attosecond lighthouses: How to use spatiotemporally coupled light fields to generate isolated attosecond pulses, Phys. Rev. Lett. **108**, 113904 (2012).
[25] J. A. Wheeler, A. Borot, S. Monchocé, H. Vincenti, A. Ricci, A. Malvache, R. Lopez-Martens, and F. Quéré, Attosecond lighthouses from plasma mirrors, Nat. Photonics **6**, 829 (2012).
[26] T. D. Arber *et al.*, Contemporary particle-in-cell approach to laser-plasma modelling, Plasma Phys. Control. Fusion **57**, 113001 (2015).
[27] See Supplemental Material at http://link.aps.org/supplemental/10.1103/PhysRevLett.133.045001 for discussions on (i) the robustness of this scheme, and (ii) the reflection regime.
[28] J. D. Jackson, *Classical Electrodynamics* (Wiley, New York, 1998).
[29] Y. Ping *et al.*, Absorption of short laser pulses on solid targets in the ultrarelativistic regime, Phys. Rev. Lett. **100**, 085004 (2008).
[30] P. Gibbon, *Short Pulse Laser Interactions with Matter* (Imperial College Press, London, 2005).
[31] W. L. Kruer and K. Estabrook, J × B heating by very intense laser light, Phys. Fluids **28**, 430 (1985).
[32] F. Brunel, Not-so-resonant, resonant absorption, Phys. Rev. Lett. **59**, 52 (1987).